Dynamic Response of a Top-tensioned Riser Under Vessel Motion

Decao Yin[a,*], Elizabeth Passano[a], Halvor Lie[a]
Guttorm Grytøyr[b], Kristoffer Aronsen[b], Michael Tognarelli[c], Elizbar Buba Kebadze[d]
a SINTEF Ocean, Trondheim, Norway
b Statoil, Oslo, Norway
c BP, Houston, Texas, USA
d BP Exploration Operating Company Ltd, Sunbury on Thames, UK

ABSTRACT

Model tests of a top-tensioned riser model were carried out as a part of a joint industry project, with the purpose of verifying the calculations of the riser analysis program RIFLEX. Sinusoidal motion in one direction was imposed at the top end of the riser model to simulate vessel motion. The tests were carried out in still water. Bending strain and acceleration were measured in both in-line (IL) and cross-flow (CF) directions along the riser model, so that the global response could be obtained through post-processing of the measured signals. Numerical simulations were performed and the results were compared with results from the model tests. This paper discusses interesting aspects of this comparison as well as the general dynamic behaviour of the top tensioned riser.

It was found that the dynamic responses of a top tensioned riser with vessel motion can consist of not only the in-line responses due to vessel motion at the riser top end, but also cross-flow vortex-induced vibrations (VIV) under conditions when Keulegan–Carpenter number is relatively small. Cross-flow VIV response is estimated using the VIVANA software and compared to the measured response. The main conclusion is however that the riser analysis program RIFLEX can predict the global dynamic responses sufficiently well.

KEY WORDS: Top-tensioned riser; vessel motion; vortex-induced vibration; in-line; cross-flow.

INTRODUCTION

A top-tensioned marine riser connects the offshore wellhead (WH) on the seabed and the mobile offshore drilling unit (MODU) on the free surface, conveying oil and mud. The marine riser is subject to waves, currents and motions of MODU induced by environmental loads (Yin et al., 2018).

VIV of a free-hanging riser due to vessel motion have been investigated by both experimentally and numerically (Jung et al., 2012; Kwon et al., 2015; Wang et al., 2016; Wang et al., 2017.)

Statoil and BP carried out a comprehensive model test program on drilling riser in MARINTEK's Towing Tank in February 2015. The objective was to validate and verify software predictions of drilling riser behaviour under various environmental conditions by the use of model test data. Six drilling riser configurations were tested. In the present study we only consider the simplest configuration, a top-tensioned bare riser with pinned boundary condition (Yin et al., 2018).

The present study focuses on the dynamic responses of a top-tensioned riser under vessel motions.

THEORETICAL BACKGROUND

Several key parameters are discussed and defined by Sumer & Fredsøe (1988) and Blevins (1990).

The forced harmonic motion at the top end of the riser $x(t)$ is:

$$x(t) = Asin(\omega t) = Asin(\frac{2\pi}{T}t) = Asin(2\pi ft) \tag{1}$$

where A is the oscillation amplitude, $\omega = 2\pi/T = 2\pi f$ is the angular oscillation frequency.
The oscillation velocity $\dot{x}(t)$ can be derived as:

$$\dot{x}(t) = \omega Acos(\omega t) = \frac{2\pi}{T}Acos(\frac{2\pi}{T}t) = 2\pi fAcos(2\pi ft) \tag{2}$$

Inserting the amplitude of the flow velocity, $2\pi A/T$, into the formula for the Keulegan–Carpenter number KC gives:

$$KC = \frac{VT}{L} = \frac{2\pi A}{T}\frac{T}{D} = \frac{2\pi A}{D} \tag{3}$$

where V is the oscillating velocity, D is the outer diameter of the riser.
The Reynolds number is defined as

$$Re = \frac{\dot{x}(t)D}{\nu} = \frac{2\pi AD}{\nu T}cos(\frac{2\pi}{T}t) = \frac{2\pi fAD}{\nu}cos(2\pi ft) \tag{4}$$

$$Re_{max} = \frac{\dot{x}_{max}D}{\nu} = \frac{2\pi AD}{\nu T} = \frac{2\pi fAD}{\nu} \tag{5}$$

where ν is the kinematic viscosity of the fluid.
The reduced velocity V_r is defined by

$$V_r = \frac{\dot{x}_{max}}{Df_n} = \frac{2\pi Af}{Df_n} = \frac{2\pi A}{D}\frac{f}{f_n} \tag{6}$$

where f_n is the measured natural oscillation frequency in still water .

MODEL TEST

The model tests have been performed in the Towing Tank III at MARINTEK (now SINTEF Ocean). The Towing Tank III has a dimension of $L \times B \times D = 85\ m \times 10.5\ m \times 10\ m$. It is equipped with a double flap wave-maker and a overhead towing carriage. The model tests to be analysed in this paper is carried out in still water.

Figure 1 shows the overview of the model test set-up. A steel truss beam is used to connect the lower end of the riser model and to the carriage. On the top side, steel substructures are added to enhance the stiffness of the rig and accommodate the horizontal oscillator. On the bottom side of the rig, four chains were spread diagonally to keep the rig vertical and provide stiffness. The truss beam is hinged on to the vertical beams, and it can be lifted to a horizontal position by the crane on the towing carriage.

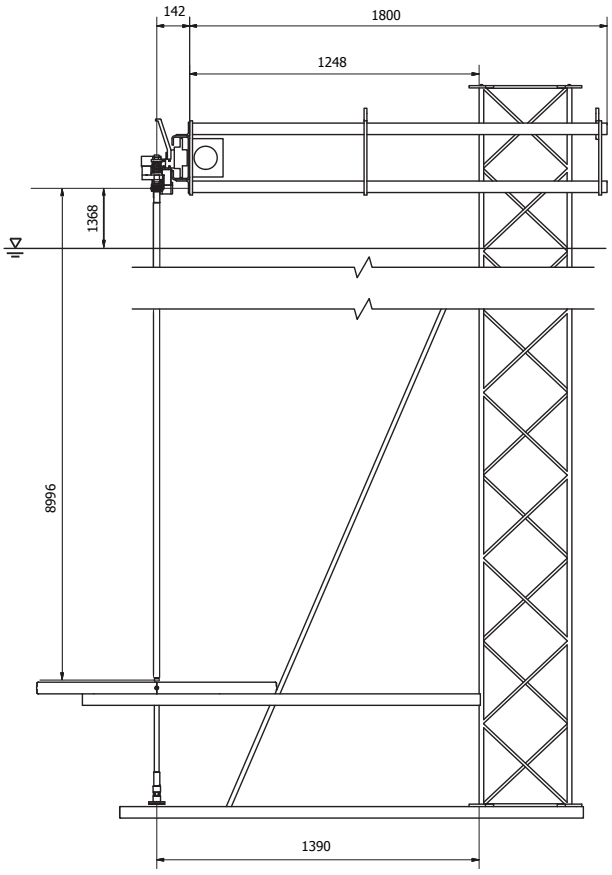

Fig. 1 Model test set-up.

The riser model is pinned on both ends, and it is pre-tensioned by a compress spring on the top end. Harmonic motion is imposed on the top end by a linear motion system, see Fig. 2. The submerged part of the riser model is filled with fresh water.

The core of the bare riser model was a fibreglass reinforced pipe. This core fibreglass pipe has an outer diameter of 20 *mm* and a wall thickness of 1.5 *mm*. It was fabricated by a subcontractor, Vello Nordic AS. The optical fibres, accelerometers, and their cables were glued on the outer surface of the fibreglass pipe. A silicon tube was wrapped around the sensors and cables. Due to the cables and silicon tube, the outer diameter of the riser model was increased to 28 *mm* generally. At the locations of accelerometers, the outer diameter was slightly larger locally.

The properties of the riser model in model scale (MS) and corresponding full scale (FS) values are summarized in Tab. 1. The drilling riser model is in 1:19 scale, and Froude scaling is applied in the present study.

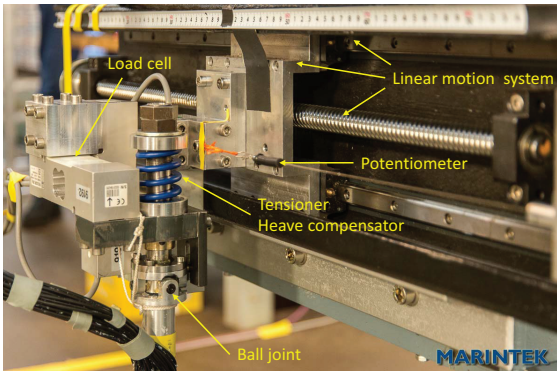

Fig. 2 Riser top unit: One degree-of-freedom (DOF) forced motion actuator, tensioner/heave compensator, ball joint, horizontal potentiometer, and three component load cell.

Table 1 Riser model properties.

Property	Unit	MS	FS
Outer diameter, OD	m	0.028	0.532
Inner diameter, ID	m	0.017	0.323
Length, L	m	8.996	171
Mass/length, m/l	kg/m	0.668	247
Bending stiffness, EI	Nm^2	120	3.5×10^8
Spring stiffness, K	N/m	1.819×10^5	6.73×10^7
Top tension, T	N	212	1.5×10^6

The bare riser model was instrumented at thirteen locations with four fibre optics strain gauges at each location. This implies 52 strain sensors. They are used to measure axial stress and biaxial bending stresses. The fibres were glued on the glass fibre rod, in four quadrants of the cross section. The fibres were protected by the outer silicon layer. Two normal strain gauges were instrumented. One is located on the bare riser top part, above the water line. One is located near the lower end of the riser. Twelve two dimensional accelerometers are instrumented on the bare riser. The fibre optic strain signals were sampled at a rate of 25 Hz. All other signals were sampled at a rate of 200 Hz. Figure 3 presents the distribution of accelerometers, fibre optic strain gauges, and strain gauges.

The displacement is obtained by integrating acceleration signals measured by accelerometers. The curvature are directly measured by both fibre optic strain gauges and normal strain gauges.

The tests studied in this paper are listed in Tab. 2. Harmonic motions at wave frequencies are imposed on the top end of the riser model. The excitation frequency is either the 1^{st} eigenfrequency (Test 1015, Test 1020 and Test 1025) or the 2^{nd} eigenfrequency (Test 1005, Test 1010 and Test 1011). Various excitation amplitudes are applied.

NUMERICAL SIMULATION

The top-tensioned riser model is numerically modelled using the riser analysis software - RIFLEX (RIFLEX 4.10.0 Theory Manual.). RIFLEX simulation is performed under the software workbench - SIMA (SIMA 3.4 User's Guide.).

Eigenvalue analysis is performed to find the eigenfrequencies and corresponding eigenmodes. Non-linear time domain global dynamic analysis is performed in in-line direction (direction of oscillation) to simulate the dynamic response in in-line direction.

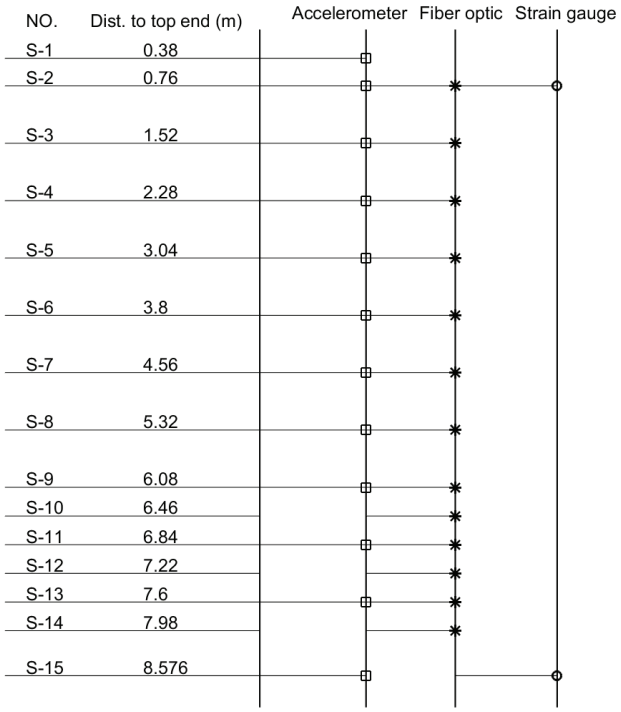

Fig. 3 Instrumentation distribution.

Table 2 Test program.

Test No.	A (m) MS/FS	T (s) MS/FS	KC_{max}	Re_{max}
1005	0.026/0.50	0.677/2.951	5.83	5.93×10^3
1010	0.052/1.00	0.677/2.951	11.67	1.18×10^4
1011	0.013/0.25	0.677/2.951	2.92	2.96×10^3
1015	0.026/0.50	1.547/6.746	5.83	2.59×10^3
1020	0.052/1.00	1.547/6.746	11.67	5.19×10^3
1025	0.078/1.50	1.547/6.746	17.50	7.87×10^3

To investigate and simulate the VIV in cross-flow direction due to oscillatory flow, VIV analysis software VIVANA (VIVANA 4.10.0 Theory Manual.) is used.

RESULTS AND DISCUSSIONS

The first three normalized eigenvector shapes found from eigenvalue analysis in RIFLEX are shown in Fig. 4. Corresponding calculated eigenfrequencies are compared with measured eigenfrequencies from still water decay test, see Tab. 3. The difference between calculated and measured eigenfrequencies are within 5 %.

Table 3 Comparison of eigenperiod.

Eigenperiod (s)	T_1	T_2	T_3
Model test	1.547	0.677	0.382
Numerical simulation	1.543	0.692	0.399

Figure 5 to Fig. 10 show the displacement response of all tests. In each figure, the plot on the left presents the dimensionless displacement amplitude along the riser model in both IL and CF directions. The plots on the two right columns show the orbits of 12 cross sections with accelerometers (check against with Fig. 3). The plots below shows the power spectral density (PSD) along the pipe model in both directions.

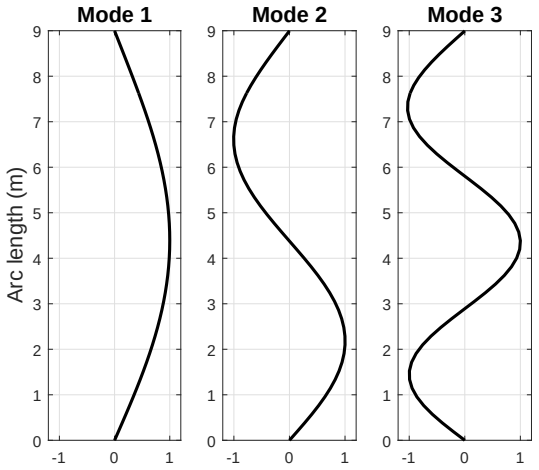

Fig. 4 Eigenmodeshapes of displacement.

Fig. 5 to Fig. 7 show a combination of 2^{nd} mode of IL response and 3^{rd} mode of CF response. Fig. 8 to Fig. 10 show a combination of 1^{st} mode of IL response and 2^{nd} mode of CF response. Further discussions will prove this. It is discovered that the accelerometer at S-6 in IL direction does not work properly for Test 1015, Test 1020 and Test 1025, it can be see from Fig. 8 to Fig. 10. The exact reason was unclear, but it was suspected that it was not perfectly water-proofed.

IL and CF responses

Even though the forced motion is only applied in the IL direction (see Tab. 2), displacements are seen in both IL and CF directions. The riser model moves at the forced motion frequency in the IL direction. In the CF direction, the motion is around double of the forced motion frequency, with several other frequencies additionally, see Tab. 4, Fig. 5(b), Fig. 7(b), Fig. 8(b), Fig. 9(b) and Fig. 10(b). Multiple frequencies in CF displacement responses result in complicated cross-sectional oscillation orbits, see Fig. 5(a) and Fig. 7(a). Single frequency displacement responses will give '8-shape' orbits, see Fig. 6(a).

Table 4 Response frequency.

Test	V_r	$f_{IL} = f$	f_{CF}	$f_{CF,l}$
1005	13.3	1.48	2.77	0.18, 1.48
1010	26.7	1.48	2.95	1.48, 0.22
1011	6.7	1.48	2.67	0.29, 1.48
1015	5.8	0.65	1.29	0.65
1020	11.7	0.65	1.29	0.65
1025	17.5	0.65	1.28	0.65, 1.75, 0.83, 0.45, 0.18

The dominating CF response frequency (VIV frequency) is double of the IL motion frequency for all six cases. The relationship between CF vibration frequency and the oscillatory flow frequency was defined by Sumer and Fredsøe (1988).

$$N = \frac{f_{CF}}{f} = \frac{f_{CF} DKC}{\dot{x}_m} \tag{7}$$

where N is the number of vibrations in one cycle of oscillating flow, $\dot{x}_m$ is the amplitude of the oscillating velocity.

If we insert the corresponding values of Test 1010 into Eq. 7, we will get $N = 2$. It is noted that the response pattern for a constant KC number varies with the reduced velocity.

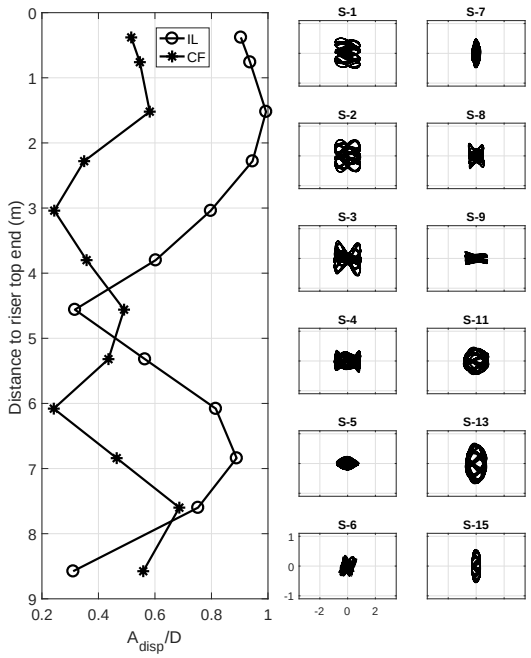

(a) Measured displacement amplitude along the riser model and orbits at locations with accelerometers.

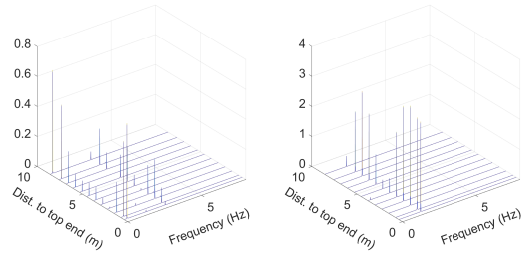

(b) PSD of displacements in CF (left) and IL (right) directions.

Fig. 5 Test 1005, $A = 0.026\ m$, $T = 0.677\ s$.

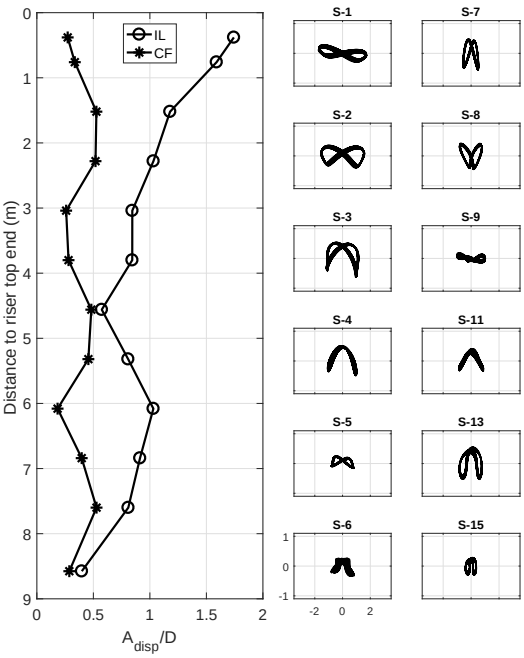

(a) Measured displacement amplitude along the riser model and orbits at locations with accelerometers.

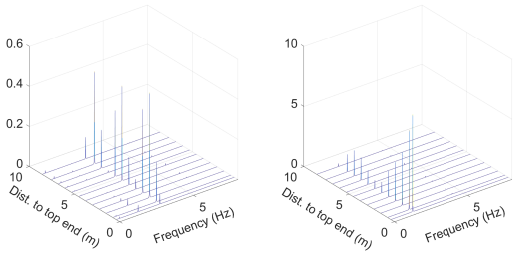

(b) PSD of displacements in CF (left) and IL (right) directions.

Fig. 6 Test 1010, $A = 0.052\ m$, $T = 0.677\ s$.

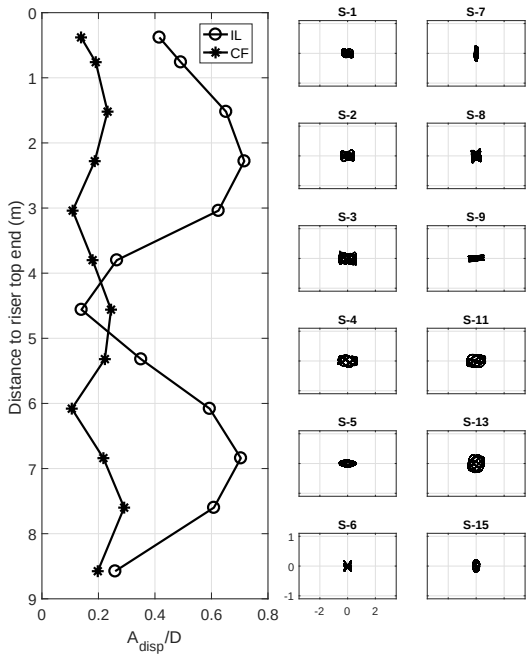

(a) Measured displacement amplitude along the riser model and orbits at locations with accelerometers.

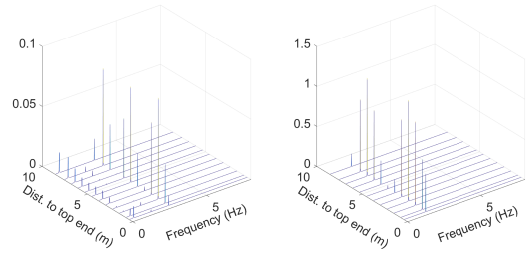

(b) PSD of displacements in CF (left) and IL (right) directions.

Fig. 7 Test 1011, $A = 0.013\ m$, $T = 0.677\ s$.

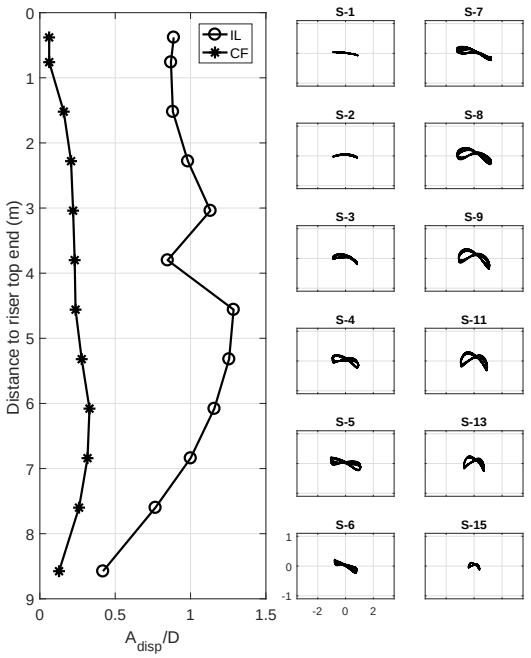

(a) Measured displacement amplitude along the riser model and orbits at locations with accelerometers.

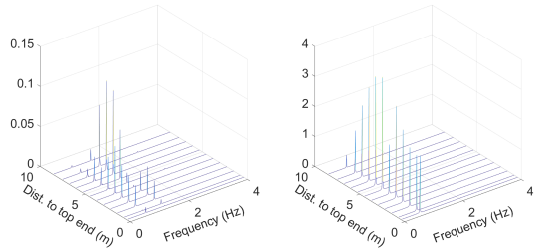

(b) PSD of displacements in CF (left) and IL (right) directions.

Fig. 8 Test 1015, $A = 0.026\ m$, $T = 1.547\ s$.

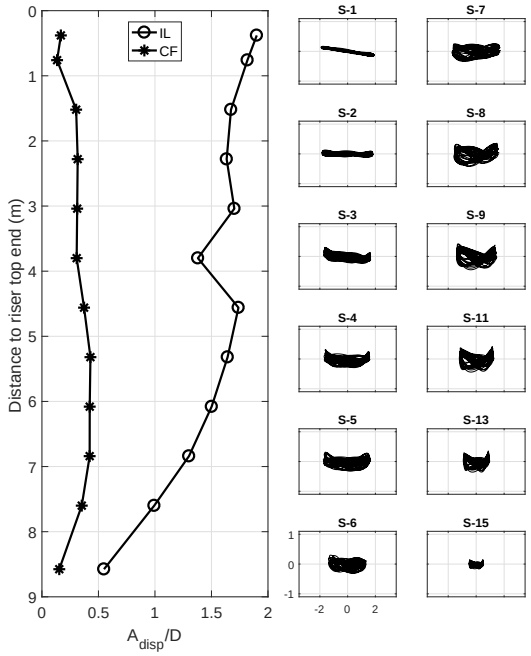

(a) Measured displacement amplitude along the riser model and orbits at locations with accelerometers.

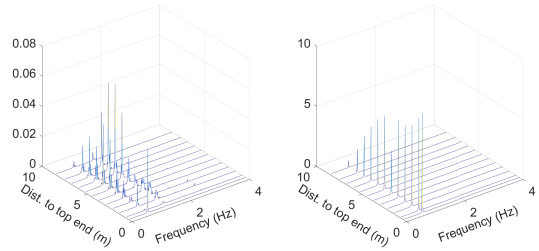

(b) PSD of displacements in CF (left) and IL (right) directions.

Fig. 9 Test 1020, $A = 0.052\ m$, $T = 1.547\ s$.

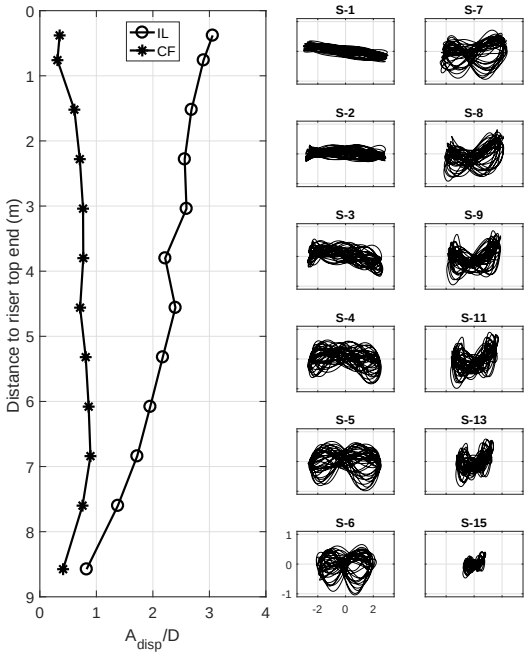

(a) Measured displacement amplitude along the riser model and orbits at locations with accelerometers.

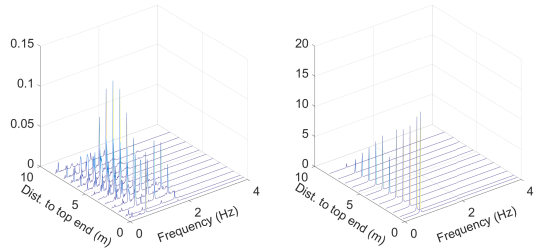

(b) PSD of displacements in CF (left) and IL (right) directions.

Fig. 10 Test 1025, $A = 0.078\ m$, $T = 1.547\ s$.

It is important to note that the KC number decreases to zero along the drilling riser from the top end to the bottom end. When KC number is smaller than 4, the force in CF direction is minimal (Blevins, 1990). That explains the multiple frequencies in CF for Test 1005 and 1011, see Tab. 4, Fig. 5(a) and Fig. 7(a). For Test 1010 (Fig. 6(a)), the maximum KC number is 11.67, vortex pairs are shed alternately into the wake during each half-cycle of oscillation, resulting distinct CF forces which has twice the frequency of IL oscillation, see Tab. 4.

The measurement signals of S-3 of Test 1010 is plotted in Fig. 11, together with the top motion history. In general, all the test cases have relatively low KC number (<20), Test 1010 has a KC number of 11.67, see Tab. 2. We can see that the CF responses are stable, without amplitude modulation. Similar responses were discovered at small KC number in Fu et al. (2014). It is probably due to that at small KC number, the vortex shedding is strengthened by its wake.

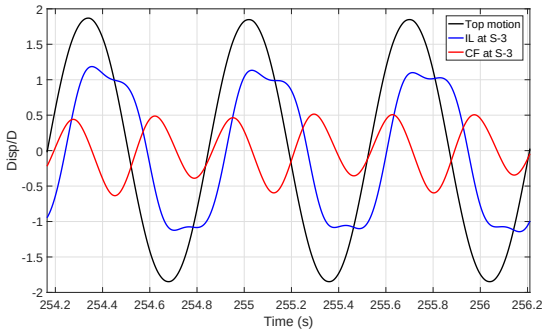

Fig. 11 Time history within 3 cycles of Test 1010, at S-3.

In-line response amplitude comparison

IL displacement amplitude comparison is shown in Fig. 12. IL curvature amplitude comparison is shown in Fig. 13. From both figures, the second mode responses are observed for Test 1005, Test 1010 and Test 1011; while the other three tests have IL responses dominated by the first mode. RIFLEX simulation over-predict both displacements and curvatures slightly, which gives conservative estimation.

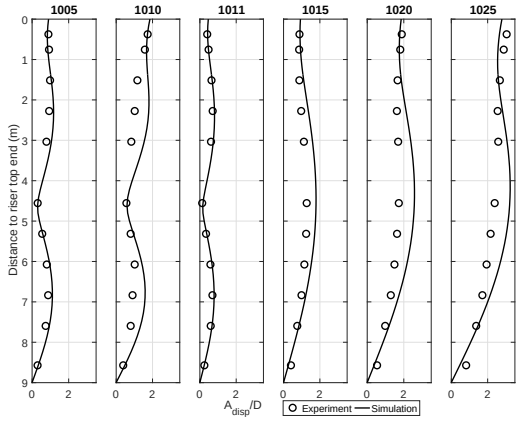

Fig. 12 Comparison of IL displacement amplitude.

The curvature amplitude comparison in Fig. 13, on the lower part of the riser (6 to 8 m from the riser top end), larger differences are observed for the first three tests. The experimental measurements indicate higher mode curvature may exist in addition to the primary mode curvature signal, however, RIFLEX seems only capture the dominating mode curvature.

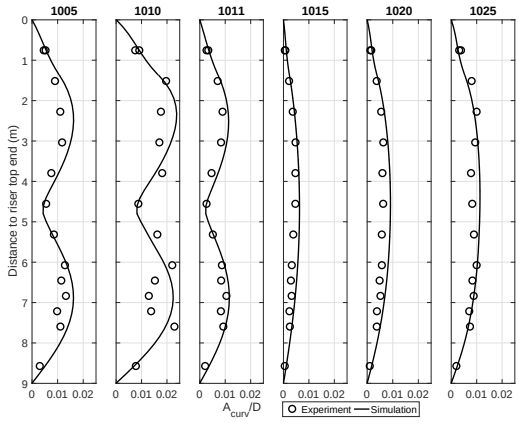

Fig. 13 Comparison of IL curvature amplitude.

Cross flow VIV responses

To study the CF VIV, time domain model developed by Thorsen and Sævik (2017) is used. It is based on Morison's equation, with an additional term representing the lift from vortex shedding. The magnitude of the vortex shedding force is given by a dimensionless coefficient, Cv, and a value of 1.3 is adopted in this study. The drag coefficient has a value of 1.0 in this study. This model allows time varying flow around the structures, it has been validated against some experiments with oscillating flow (Thorsen et al, 2016). The synchronization model within the hydrodynamic load model is able to capture the vortex shedding process in oscillatory flow. It is important to note that the present time domain model only predict the CF VIV responses.

Selected results are presented in Fig. 14, Fig. 15 and Fig. 16.
Figure 14 shows the time history of the IL and CF responses at S-3 together with the top motion, in addition, spectral analysis is shown in the lower plot in the same figure. It is observed that dominating frequency of the CF VIV responses is double of the IL forced motion frequency, which agrees very well with the experimental measurements, see Tab. 4. In addition, strong low frequency component is also observed, which causes that the CF VIV responses have non-zero mean position.

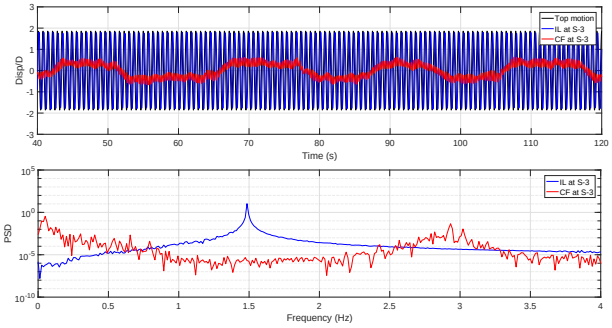

Fig. 14 Time domain CF VIV simulation results: time history of top motion and IL and CF motions at S-3 (upper), spectral analysis (lower).

Time history within three cycles of two separate time windows are presented in Fig. 15 and Fig. 16. If we look at the predicted CF VIV responses, Fig. 15 has positive mean value, while Fig. 16 has negative mean value. Moreover, the phase angle between the IL and CF motions are shifted with 180 degrees. Such phase shift was not observed in the experiments. Further studies are needed to investigate whether it is physical or numerical. The predicted amplitude is not very good, but this can be probably be improved by modifying the

excitation and damping parameters.

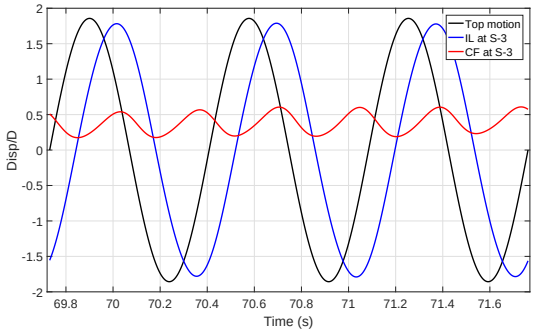

Fig. 15 Time domain CF VIV simulation results within 3 cycles of Test 1010, at S-3, selected time window 1.

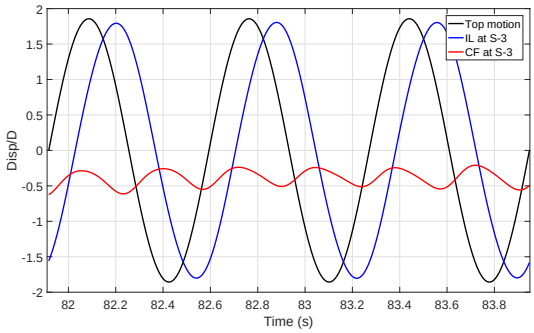

Fig. 16 Time domain CF VIV simulation results within 3 cycles of Test 1010, at S-3, selected time window 2.

CONCLUSIONS

A comprehensive drilling riser model test program was performed by a Joint Industry Project funded by Statoil and BP. The model tests were carried out at MARINTEK's towing tank (now SINTEF Ocean) extension in February 2015. Six drilling riser configurations were modelled and tested, this paper studies the configuration which is a pin-pined bare riser model. One DOF harmonic horizontal forced motions were imposed on the top end of the riser model by an actuator. Bending strain along the drilling riser model in both In-line and cross-flow directions were measured by strain gauges, accelerations in both directions were measured by accelerometers. Forces were measured at specific locations. The model tests have simplified but well-defined drilling riser models, covering extensive environmental conditions. The model test data forms a good database, which can be used in many ways, and these help to further understand the complicate responses of typical drilling risers.

The IL responses are induced by the top motion. Eigen-value analysis and non-linear time domain analysis have been carried out by using a riser system analysis program RIFLEX. Key results such as displacement and curvature amplitudes along the riser from model tests are compared with the numerical simulations. Orbits at measurement locations and spectral analysis results along the riser are presented in addition. In most of the selected cases, RIFLEX over-predicts the displacement and curvature amplitude, indicating conservative prediction.

Responses in CF direction are measured, which are caused by vortex-induced vibrations in oscillatory flow. The test cases have relative small KC number, the VIV responses are stable. Even the amplitude of CF VIV response is much smaller than the IL responses, since the frequency is double as the IL frequency, the VIV responses in CF may cause significant fatigue damage. A recently developed time domain VIV prediction tool is applied to simulate the CF VIV caused by the harmonic IL top motion. The result is promising, the CF VIV amplitude and frequency are predicted correctly. Further studies are needed to investigate the phase shift in the numerical simulation. The predicted amplitude could be improved by modifying the excitation and damping parameters.

ACKNOWLEDGEMENTS

The authors would like to thank Statoil and BP for their support and allowing the publication of the present paper, their contribution and comments on this study are highly appreciated.

REFERENCES

Blevins, R. D. (1990). "Flow-Induced Vibration", Van Nostrand Reinhold, New York.

Fu, S., Wang, J., Baarholm, R., Wu, J., & Larsen, C. M. (2014). "Features of vortex-induced vibration in oscillatory flow", ASME. J. Offshore Mech. Arct. Eng., 136(1), pp. 011801–011801–10.

Jung, D., Lee, H., Kim, H., & Moon, D. (2012). "Study of Vortex-Induced Vibrations in a Riser under Low Keulegan–Carpenter numbers", Proceedings of the Twenty-second (2012) International Ocean and Polar Engineering Conference, Rhodes, Greece.

Kaasen, K. E., Lie, H., Solaas, F., & Vandiver, J. K. (2000). "Norwegian Deepwater Program: Analysis of Vortex-Induced Vibrations of Marine Risers Based on Full-Scale Measurements", Offshore Technology Conference., Houston, Texas, USA.

Kwon, Y. J., Kim, H. J., & Jung, D. H. (2015). "A study for forced oscillation experiment for OTEC riser under current", Proceedings of the Twenty-fifth (2015) International Ocean and Polar Engineering Conference, Kona, Hawaii, USA.

SINTEF Ocean. (2017). "RIFLEX 4.10.0 Theory Manual", Trondheim, Norway.

SINTEF Ocean. (2017). "SIMA 3.4 User's Guide", Trondheim, Norway.

SINTEF Ocean. (2017). "VIVANA 4.10.0 Theory Manual", Trondheim, Norway.

Sumer, B. M., & Fredsøe, J. (1988). "Transverse vibrations of an elastically mounted cylinder exposed to an oscillating flow", ASME. J. Offshore Mech. Arct., 110, pp. 387–394.

Thorsen, M. J., Sævik, S. (2017). "Simulating Riser VIV in Current and Waves Using an Empirical Time Domain Model", ASME. International Conference on Offshore Mechanics and Arctic Engineering, Trondheim, Norway.

Thorsen, M. J., Sævik, S., Larsen, C.M. (2016). "Time domain simulation of vortex-induced vibrations in stationary and oscillating flows", Journal of Fluids and Structures, 61, pp. 1–19.

Wang, J., Joseph, R., Ong, M., & Jakobsen, J. (2017). "Numerical Investigation on Vessel Motion-Induced VIV for a Free Hanging Riser Under Small Keulegan-Carpenter Numbers", Proceedings of ASME. International Conference on Offshore Mechanics and Arctic Engineering, Trondheim, Norway.

Wang, J., Xiang, S., Fu, S., Cao, P., Yang, J., & He, J. (2016). "Experimental investigation on the dynamic responses of a free-hanging water intake riser under vessel motion", Marine Structures, 50, pp. 1–19.

Wang, J. (2017). Private Communication.

Wu, J. (2017). Private Communication.

Yin, D., Lie, H., Russo, M., & Grytøyr, G. (2018). "Drilling riser model tests for software verification", ASME. J. Offshore Mech. Arct. Eng., 140(1), pp. 011701–011701–15.